Anchoring Ultrafine Metallic and Oxidized Pt Nanoclusters on Yolk-Shell TiO_2 for Unprecedentedly High Photocatalytic Hydrogen Production

Jun Jin,[a] Chao Wang,[a] Xiao-Ning Ren,[a] Shao-Zhuan Huang,[a] Min Wu,[a] Li-Hua Chen,[a] Tawfique Hasan,[b] Bin-Jie Wang,[c] Yu Li[a, *] and Bao-Lian Su[a, d, e, *]

[a]*Laboratory of Living Materials at the State Key Laboratory of Advanced Technology for Materials Synthesis and Processing, Wuhan University of Technology, 122 Luoshi Road, 430070 Wuhan, Hubei, China; Email: yu.li@whut.edu.cn and baoliansu@whut.edu.cn*

[b]*Cambrige Graphene Centre, University of Cambridge, 9 JJ Thomson Avenue, Cambridge, CB3 0FA, United Kingdom.*

[c]*FEI Company, Shanghai Nanoport, 399 Shengxia Road, 201210 Shanghai, China.*

[d]*Laboratory of Inorganic Materials Chemistry (CMI), University of Namur, 61 rue de Bruxelles, B-5000 Namur, Belgium; E-mail: bao-lian.su@unamur.be*

[e] *Clare Hall, University of Cambridge, United Kingdom; E-mail: bls26@cam.ac.uk*

Abstract: We demonstrate an alkali modification process to produce highly dispersed ultrafine Pt nanoclusters with metallic Pt^0 and oxidized Pt^{2+} species as co-catalyst anchored on nanosheet-constructed yolk-shell TiO_2 ($NYTiO_2$-Pt) acting as light harvesting reactor for highly efficient photocatalytic H_2 production. Benefiting from the high surface area, highly dispersed ultrafine Pt nanoclusters (~0.6 nm) with Pt^0 and Pt^{2+} species and special nanosheet-constructed yolk-shell structure, this novel light harvesting reactor exhibits excellent performance for photocatalytic H_2 production. The $NYTiO_2$-Pt-0.5 (0.188 wt% Pt) demonstrates an unprecedentedly high H_2 evolution rate of 20.88 mmol h^{-1} g^{-1} with excellent photocatalytic stability, which is 87 times than that of $NYTiO_2$-Pt-3.0 (0.24 mmol h^{-1} g^{-1}, 1.88 wt% Pt), and also much higher than those of other TiO_2 nanostructures with the same Pt content. Such H_2 evolution rate is the highest reported for photocatalytic H_2 production with such a low Pt content under simulated solar light. Our strategy here suggests that via alkali modifying the photocatalysts, we can not only enhance the H_2 production for solar energy conversion but also significantly decrease the noble metal content for cost saving.

Keywords: Nanosheet-constructed yolk-shell TiO_2; alkali modification; Pt nanoclusters; Pt^0 and Pt^{2+}; photocatalytic H_2 production.

Introduction

Solar-driven photocatalysis for hydrogen production from renewable resources has attracted a tremendous interest as a promising approach for clean energy generation and environmental remediation in recent years.[1, 2] Generally, for H_2 production using a semiconductor, the conduction band (CB) edge should be more negative than $E(H^+/H_2)$ (0 V at pH 0), while the valence band (VB) edge should be more positive than $E(O_2/H_2O)$ (1.23 V at pH 0).[3] Using this criterion, thus far, various photocatalysts (such as TiO_2, ZnO, CdS, ZnS, MoS_2, $BiWO_3$, g-C_3N_4) have been developed for hydrogen production.[4-13] And these photocatalysts are often co-catalysed or modified by non-metals,[14] other semiconductors,[15-18] non-noble metals[19] and noble metals[20, 21] to turn their electronic band gaps and address the rapid recombination of photogenerated electron-hole pairs.

Amongst these strategies proposed to enhance photocatalytic H_2 production, noble metal (such as Pt, Pd, Au, Ag and Rh) deposition as co-catalyst has been proven to be an effective method for photocatalytic H_2 production enhancement (without cost consideration) because they exhibit high affinity to photogenerated electrons in CB of many photocatalysts.[22] In particular, Pt is considered as the most effective noble metal for H_2 production due to its photostability with the lowest overpotential and largest work function.[23] Generally, it is essential to create Schottky barriers between Pt and photocatalyst. When a Fermi level equilibration is achieved, interfacial charges quickly transfer to Pt through the metal-semiconductor heterojunction, resulting in the reduction of H^+ and formation of H_2 on Pt.[24] This means that the size, dispersion and content of Pt on to photocatalysts have a

significant effect on the photocatalytic H_2 production activity of Pt-deposited photocatalyst.[24, 25] Thus it is critical to employ appropriate synthetic routes for the deposition of uniformly dispersed ultrafine Pt nanoparticles on to photocatalysts for highly improved H_2 production. Recently, Li *et al.* have reported isolated single-atom Pt as co-catalyst in 2D g-C_3N_4 to change the intrinsic surface trap states for a highly efficient photocatalytic H_2 production, due to a longer lifetime of photogenerated electrons caused by the isolated single Pt atom.[26] This method is effective to embed single-atom Pt in g-C_3N_4 due to the only carbon and nitrogen. However, the posibility of co-catalysing single Pt atom in metal oxides-based photocataysts is unclear. Indeed, anchoring ultrafine Pt nanoparticles on these metal oxides-based photocatalysts is still a big challenge.

In this context, wet-chemistry reduction of H_2PtCl_6 has already offered the opportunity for Pt nanoparticles deposition as co-catalysts for photocatalytic enhancement.[27-30] Recently, Zhai *et al.* have reported that alkali modification of Pt can induce Pt nanoparticles with alkali-$O_x(OH)_y$ species loaded on alumina or silica, which are active at the low-temperature for H_2 production via water-gas shift reaction both in experiment and in density functional theory calculations.[31] We then reasonably suppose that alkali modification has the same effect on improving the amount of the surface bridging hydroxyls on the surface of both metal oxides-based photocatalysts and Pt nanoparticles. And the surface bridging hydroxyls on the metal oxides-based photocatalyst may increase the active sites for Pt deposition and promote uniform deposition of ultrafine Pt nanoparticles (or even nanoclusters). This also decreases the content of Pt for cost saving. Further, in the alkali

modification reaction process, the reduction of H_2PtCl_6 can be retarded. This may induce Pt^{2+} species within the Pt nanoparticles (or nanoclusters) to effectively prevent the backward reaction of H_2 and O_2.[24]

Herein, we choose a hierarchical nanosheet-constructed yolk-shell TiO_2 ($NYTiO_2$) microsphere as model photocatalyst for alkali modification. On one hand, TiO_2 is considered as one of the most promising photocatalysts for water splitting due to its superior photocatalytic properties, abundance, non-toxicity and photostability.[32-34] On the other hand, such hierarchically yolk-shell structure with high surface area and low density can enhance light harvesting efficiency through multiple reflections of incident light and provide short diffusion paths for photogenerated electrons.[34, 35] In addition, the nanosheets are suitable for ultrafine Pt deposition and uniform distribution. Then, a simultaneous NaOH-modification and $NaBH_4$-reduction of Pt is adopted. This leads to the synthesis of the alkali modified Pt nanoclusters in $NYTiO_2$ light harvesting reactor (Scheme 1a). As expected, ultrafine Pt nanoclusters (~0.6 nm) with metallic Pt^0 and oxidized Pt^{2+} species are achieved and uniformly dispersed in such hierarchical $NYTiO_2$. The NaOH-modified $NYTiO_2$-Pt-0.5 (0.188 wt% Pt) light harvesting reactor demonstrates an excellent H_2 evolution rate of 20.88 mmol h^{-1} g^{-1}, 87 times that of $NYTiO_2$-Pt-3.0 (0.24 mmol h^{-1} g^{-1}, 1.88 wt% Pt) and much higher than those of other TiO_2 nanostructures with 0.188 wt% Pt. To the best of our knowledge, this represents the highest H_2 evolution ever reported under simulated solar light with such a low Pt content. Our results indicate that alkali modification of hierarchically structured porous metal oxides-based photocatalysts with Pt nanoclusters deposition is highly

efficient for photocatalytic H_2 production, and offers significant cost saving due to very low Pt content.

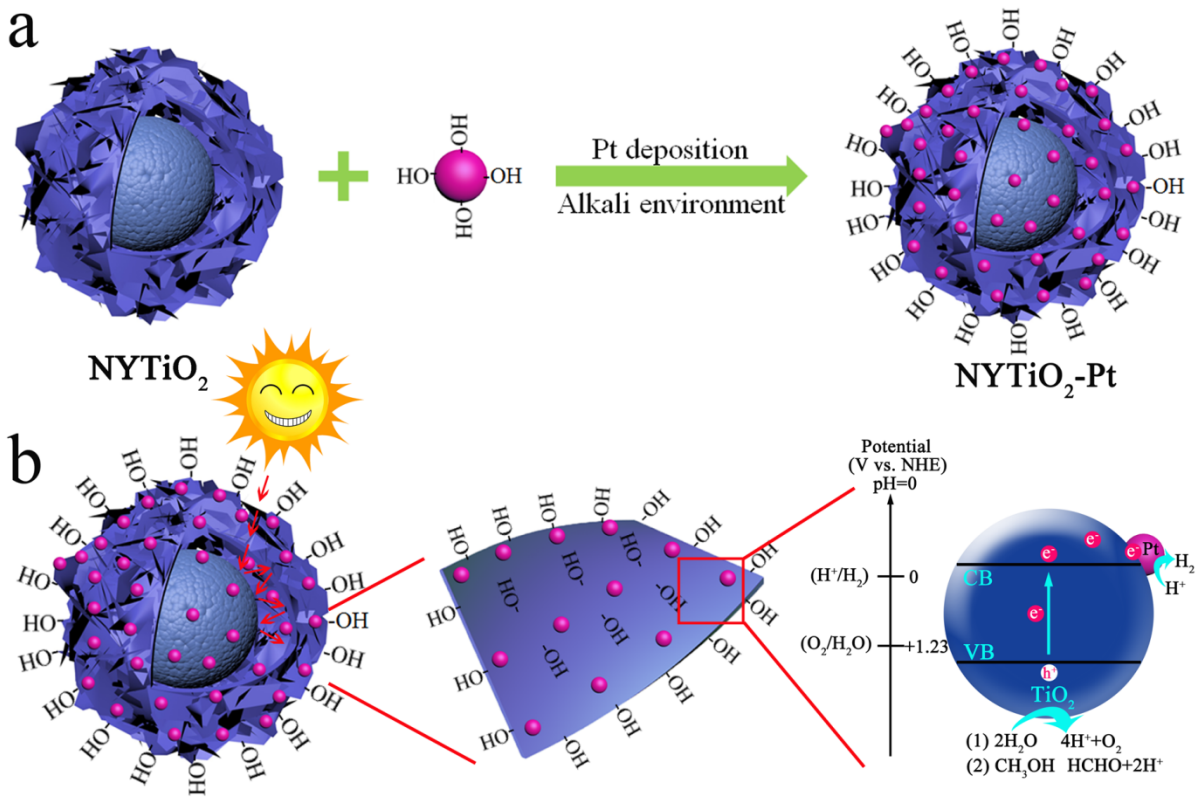

Scheme 1. (a) The Pt deposition and NaOH-modification process of $NYTiO_2$ and (b) the illustration of $NYTiO_2$-Pt light harvesting reactor for H_2 production.

Experimental Section

Materials

Titanium isopropoxide (TTIP), titanium (IV) butoxide (TBT) are purchased from Aldrich. Tetraethylenepentamine (TEPA) is purchased from Aladdin. Isopropanol, anhydrous methanol, anhydrous ethanol, sodium hydroxide (NaOH), $NaBH_4$ and KCl are purchased from Sinopharm Chemical Reagent Ltd. Co. Chloroplatinic acid ($H_2PtCl_6 \cdot 6H_2O$) is purchased

from Sigma Chemical Co. Commercial P25 is purchased from Degussa Co. Ltd. All the chemicals are used as received.

Synthesis of $NYTiO_2$

In a typical synthesis, 0.12 mL TEPA is added in to 84 mL isopropanol under stirring. Then, 3 mL of TTIP is added to the above solution and stirred for 30 minutes. The solution is then transferred into a 150 mL Teflon-lined autoclave and kept at 200 °C for 24 h. After cooled to room temperature, the precipitate is washed with ethanol via centrifugation for several times and dried at 60 °C. Finally, the $NYTiO_2$ product is obtained via calcination of the precipitate at 400 °C for 2 h.

Synthesis of $MeTiO_2$

The mesoporous TiO_2 ($MeTiO_2$) microspheres are prepared via a sol-gel synthesis. Typically, 200 mL ethanol is mixed with 0.8 mL 0.1 M KCl aqueous solution, followed by adding 5.0 mL TBT to the above mixed solution and is stirred for 30 minutes. Then the suspension is aged at room temperature for 24 h. The white precipitate is washed with ethanol for several times. Finally, the $MeTiO_2$ microspheres are obtained after calcination of the TiO_2 solid spheres at 400 °C for 2 h.

Synthesis of $NYTiO_2$-Pt photocatalysts

Typically, 200 mg $NYTiO_2$ is added into a single-necked flask containing chloroplatinic acid solution (20 mL, 0.05 mg mL^{-1}). Then 2 mL freshly prepared $NaBH_4$ aqueous solution (2 mg mL^{-1}, containing 0.5 M NaOH) is rapidly injected into the solution under vigorous magnetic stirring. After 2 h of stirring, another 2 mL freshly prepared $NaBH_4$ solution (2 mg

mL^{-1}, containing 0.5 M NaOH) is injected into the solution and stirred for 12 h. The precipitate is washed by distilled water and ethanol via centrifugation for several times. After drying at 60 °C in a vacuum oven, the NYTiO_2-Pt photocatalysts are finally obtained. The NYTiO_2-Pt photocatalysts with various Pt contents, NYTiO_2-Pt-0.25, NYTiO_2-Pt-0.5, NYTiO_2-Pt-1.0, NYTiO_2-Pt-2.0 and NYTiO_2-Pt-3.0, are synthesized through changing chloroplatinic acid concentrations of 0.025, 0.05, 0.1, 0.2 and 0.5 mg mL^{-1}, respectively. Table S1 shows the weight content of Pt. The MeTiO_2-Pt-0.5 and P25-Pt-0.5 are synthesized with the same procedure of NYTiO_2-Pt-0.5. The NYTiO_2-Pt-0.5N is also prepared with the same procedure of NYTiO_2-Pt-0.5 without NaOH in $NaBH_4$ solution.

Characterizations

Crystallographic phases of the samples are investigated by XRD on a Bruker D8 with Cu Kα radiation (λ=0.15405 nm) at 40 mA and 40 kV. The morphologies of the samples are characterized by a field-emission scanning microscopy (FESEM, Hitachi S-4800). Transmission electron microscopy (TEM), including bright field (BF) images, dark field (DF) images, HAADF-STEM images, STEM-EDS mapping images of NYTiO_2-Pt are collected on a FEI Talos-200X at 200 kV. TEM images of NYTiO_2, MeTiO_2 and P25 are collected on a JEOL JEM 2100F at 200 kV. Nitrogen adsorption-desorption isotherms are obtained using a Micromeritics surface area & porosity analyzer (TriStar II 3020). The absorption spectra are collected on with a UV-vis spectrometer (UV2550, Shimadzu). The surface electronic states of Ti, O and Pt are analyzed by X-ray photoelectron spectroscopy (XPS, VG Multilab 2000).

Evaluation of photocatalytic activity

The photocatalytic hydrogen production is performed in a glass-closed-circulation system with a top irradiation-type reaction vessel (LabSolar II H_2 production system, Perfect light, China) using a PLS-SXE-300C Xe lamp with a UV light of 34 mW cm^{-2} and visible light of 158 mW cm^{-2} at a distance of 15 cm. The temperature of reactant solution is maintained at 15 °C by a flow of cooling water during the photocatalytic process. 50 mg NYTiO_2-Pt photocatalyst is dispersed in a reaction vessel containing 50 mL of distilled water and 30 mL of methanol. The amount of H_2 is monitored on an online thermal conductivity detector (TCD) gas chromatograph (GC, Agilent 7890A).

Apparent quantum yields (AQY) defined by the following equation are measured using a PLS-SXE-300C Xe lamp with 365 nm band-pass filter (20 mW cm^{-2}) and an irradiatometer:

$$\begin{aligned} \mathrm{AQY} &= \frac{\text{Number of reacted electrons}}{\text{Number of incident photos}} \times 100 \\ &= \frac{\text{Number of evolved } H_2 \text{ molecules} \times 2}{\text{Number of incident photons}} \times 100 \end{aligned} \quad (1)$$

For the photocatalytic experiment and AQY test, 20 mg NYTiO_2-Pt-0.5 photocatalyst is dispersed in 80 mL aqueous solution containing 30 mL CH_3OH as a sacrificing agent. The amount of H_2 is also monitored on an online thermal conductivity detector (TCD) gas chromatograph (GC, Agilent 7890A).

Results and discussions

The details of the NYTiO_2 synthesis can be found in the literature.[36] Here, we briefly mention the pertaining morphological information of the NYTiO_2 microspheres obtained via X-ray diffraction (XRD), scanning electron microscopy (SEM) and transmission electron

microscopy (TEM). The outer shell (~250 nm thick; Figure S1a, b) of the anatase phase $NYTiO_2$ (Figure 1) is formed by nanosheets (Figure S1c) while the inner core (~500 nm diameter; Figure S1d, e) is constructed by aggregated small nanoparticles (Figure S1c). The shell thickness is ~250 nm and core size is ~500 nm (Figure S1e). The $NYTiO_2$ microspheres exhibit 168 m^2 g^{-1} specific surface area, 3 nm (in inner mesoporous core) and 15 nm (in outer nanosheets) dual pore sizes (Figure S2). This special yolk-shell structure with high BET surface area is beneficial for ultrafine Pt nanoclusters uniformly anchored onto TiO_2 nanosheets shell. The dual pores in this unique yolk-shell structure are helpful for light harvesting.

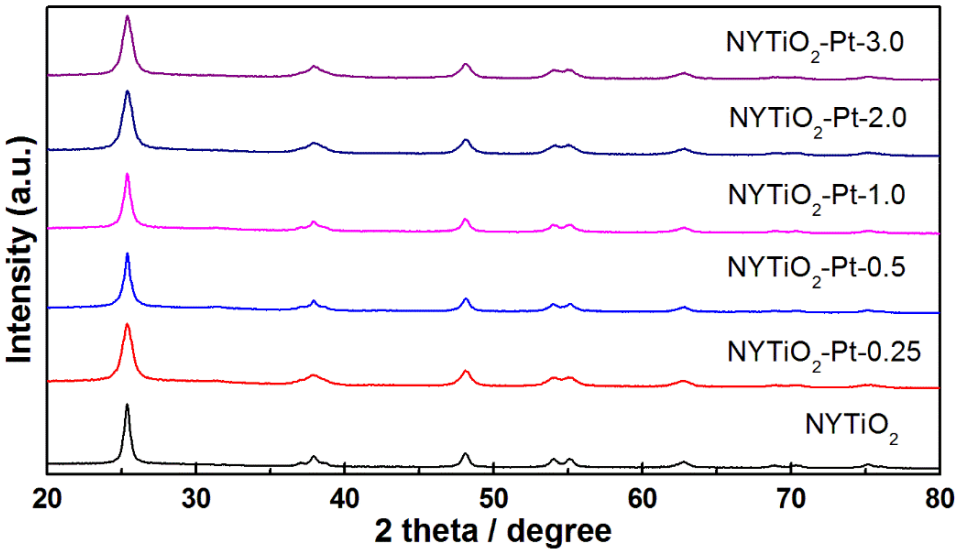

Figure 1. XRD patterns of $NYTiO_2$ and $NYTiO_2$-Pt samples with different Pt contents.

Pt nanoclusters are then deposited onto the hierarchical $NYTiO_2$ via NaOH modification (Scheme 1a). Table 1 lists the Pt content for all these samples. However, XRD results show no obvious difference for the $NYTiO_2$ and $NYTiO_2$-Pt samples (Figure 1). We believe that this is due to the very low Pt content and highly dispersed ultrafine Pt nanoclusters. Figure S3a shows the UV-Vis absorption spectra of $NYTiO_2$ and $NYTiO_2$-Pt samples. The

corresponding Tauc plots revealing the quantity hν (the energy of the light) and the quantity $(Ahν)^{1/2}$ (A is the absorption coefficient) are presented in Figure S3b. All the obtained E_g from the intercept of the tangents are similar and are listed in Table 1, indicating that there is no obvious difference on the electronic band gaps for these samples.

Table 1 The Pt contents, band gaps and H_2 rate of the $NYTiO_2$-Pt samples with/without NaOH modification and the $MeTiO_2$-Pt sample.

Sample	Pt content (wt%)	Band gap (eV)	H_2 production rate ($mmol\ h^{-1}\ g^{-1}$)
$NYTiO_2$-Pt-0.25	0.094%	2.86	14.06
$NYTiO_2$-Pt-0.5	0.188%	2.85	20.88
$NYTiO_2$-Pt-1.0	0.377%	2.86	16.50
$NYTiO_2$-Pt-2.0	0.753%	2.93	0.64
$NYTiO_2$-Pt-3.0	1.88%	2.94	0.24
$NYTiO_2$-Pt-0.5N	0.188%	2.94	5.20
$MeTiO_2$-Pt-0.5	0.188%	3.01	6.81
P25-Pt-0.5	0.188%	2.96	8.62

SEM images show that the hierarchical nanosheet-constructed yolk-shell structure can be completely retained after Pt deposition, via the chemical reduction process in an alkaline condition (Figure 2). It is interesting to note that after NaOH modification, the nanosheets-constructed shell has loosed a little comparing to the original $NYTiO_2$. In particular, many pores appear in the nanosheets after Pt nanoclusters deposition under alkali modification. These pores are also beneficial for light penetrating and harvesting. However, upon intensive SEM investigations, no Pt nanoclusters are observed in any of the $NYTiO_2$-Pt samples. Further, no signal of Pt is detected via the SEM-EDS characterization, even for $NYTiO_2$-Pt-3.0 with a high content of 1.88 wt% Pt (Figure S4). We thus reasonably conclude that the Pt nanoclusters are beyond the detection range due to their ultrafine size and uniform

deposition onto TiO_2 nanosheets.

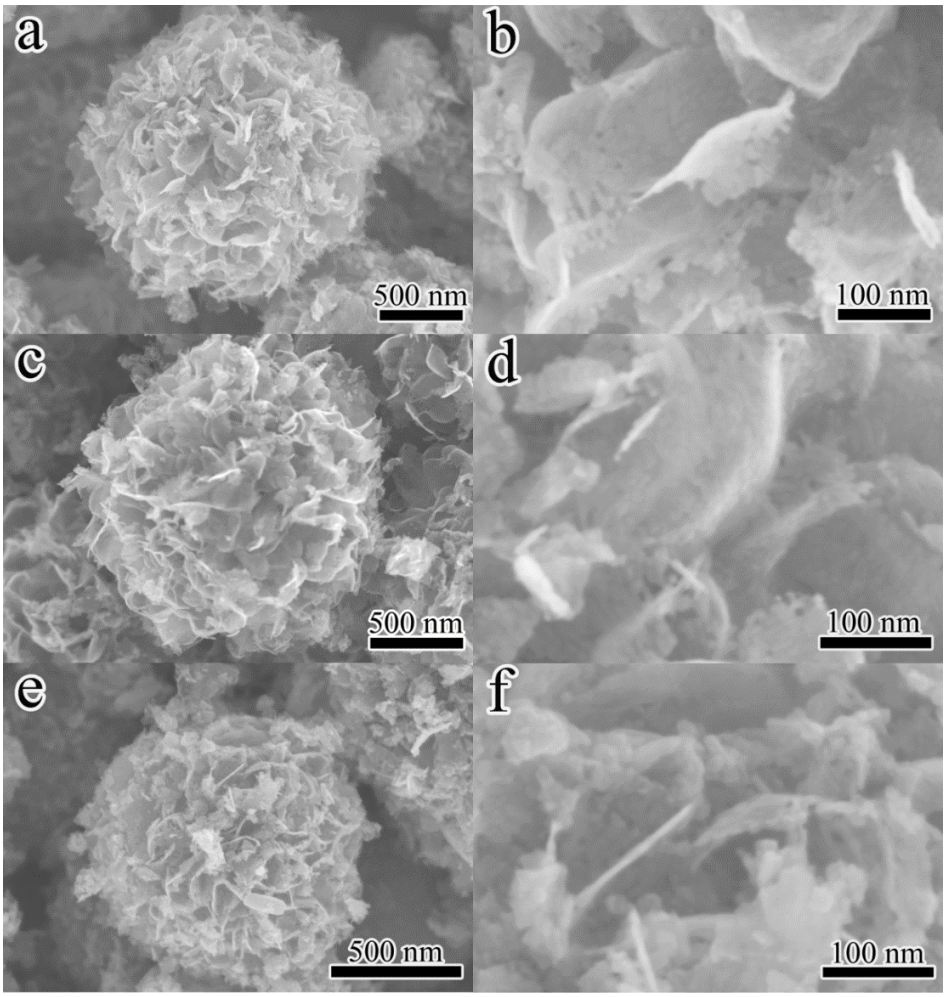

Figure 2. SEM images of $NYTiO_2$-Pt samples with different Pt contents: (a, b) $NYTiO_2$-Pt-0. 5, (c)-(d) $NYTiO_2$-Pt-1.0, (e)-(f) $NYTiO_2$-Pt-3.0.

TEM analysis is then carried out to investigate the Pt nanocluster size and distribution in the $NYTiO_2$-Pt samples. Figure 3a-c demonstrate typical bright field (BF), dark field (DF) and high angle annular dark field-scanning transmission electron microscopy (HAADF-STEM) images of $NYTiO_2$-Pt-0.5 at low magnification, respectively. These images verify the well-retained hierarchical yolk-shell structure of $NYTiO_2$ after NaOH modification and Pt deposition. Figure 3d presents a close observation of the shell. It shows several ultrafine Pt nanoclusters in $NYTiO_2$-Pt-0.5. Figure 3d inset gives the HRTEM image of one Pt

nanocluster in size of 0.8 nm. Figure 3e shows the HAADF-STEM image with a small area of the outer shell. Still, it clearly displays the highly dispersed ultrafine Pt nanoclusters in TiO_2 nanosheets. Figure 3f gives the size distribution of Pt nanoclusters from TEM images. It shows the size of the Pt nanoclusters mainly centering at ~0.6 nm.

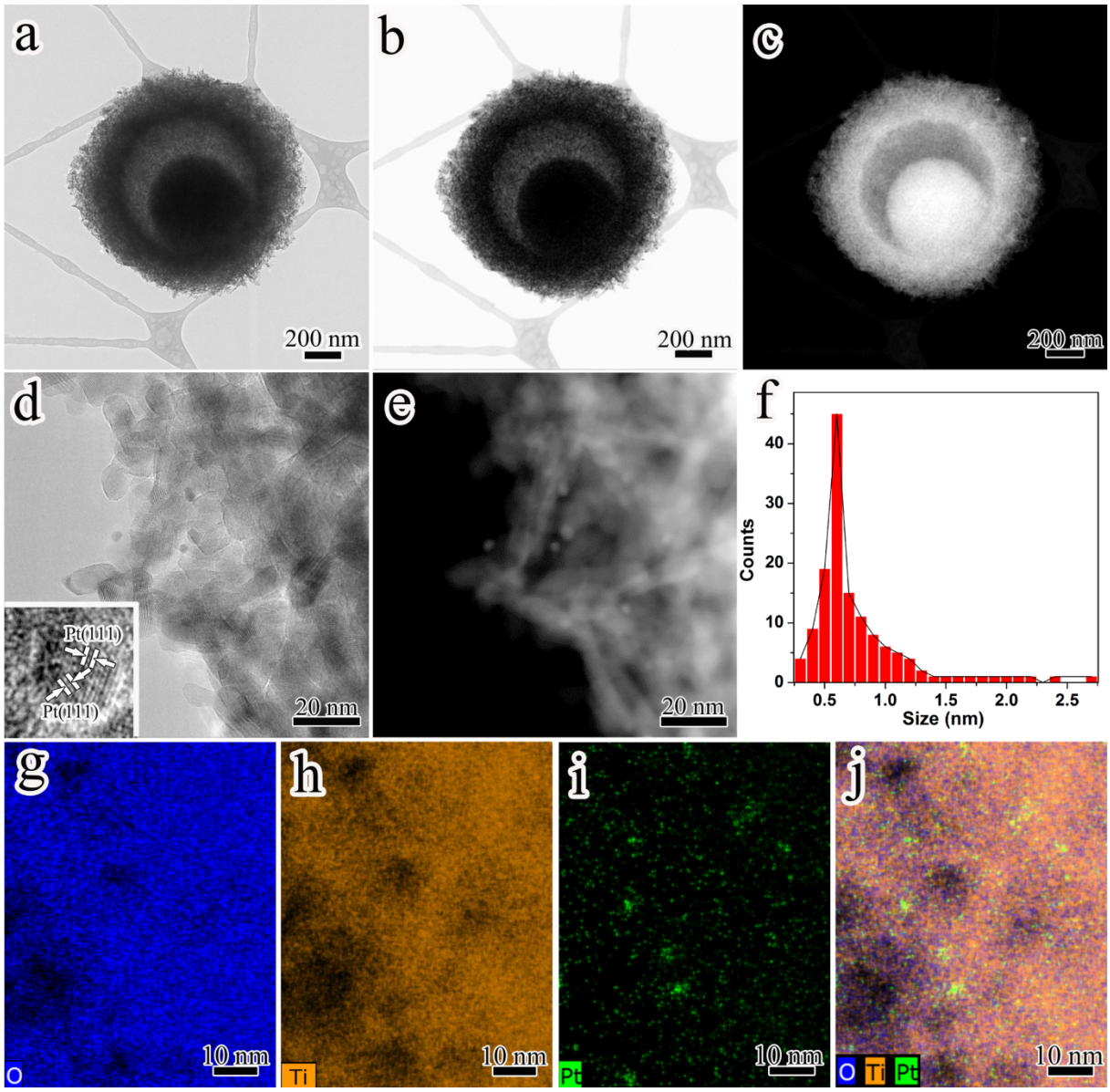

Figure 3. TEM characterizations of $NYTiO_2$-Pt-0.5. (a) BF image, (b) DF image, (c, e) HAADF-STEM images and (d) HRTEM image. The inset image in (d) is the HRTEM images of one Pt nanocluster in size of ~0.8 nm. (f) The Pt nanoparticle size distribution measured from TEM images. (g)-(j) STEM-EDS mapping images: (j) O; (k) Ti; (l) Pt; (m) whole elements.

Scanning transmission electron microscopy-electron dispersive spectroscopy (STEM-EDS) elemental mapping is further carried out to clearly show the chemical distribution of $NYTiO_2$-Pt-0.5. The elemental mapping images (Figure 3g-i) indicate the uniform distribution of O, Ti and Pt elements. Figure 3j superimposes the chemical distribution images of O, Ti and Pt elements. In particular, the uniform distribution of Pt means that the Pt nanoclusters are well dispersed in nanosheet-constructed yolk-shell structure. This is very important for photocatalytic H_2 production enhancement and also for cost saving. Figure S5 also presents the HAADF-STEM and STEM-EDS images of $NYTiO_2$-Pt-3.0, indicating the well dispersed Pt nanoclusters. Figure S5c shows the size of Pt nanoclusters in $NYTiO_2$-Pt-3.0, similar to that of $NYTiO_2$-Pt-0.5.

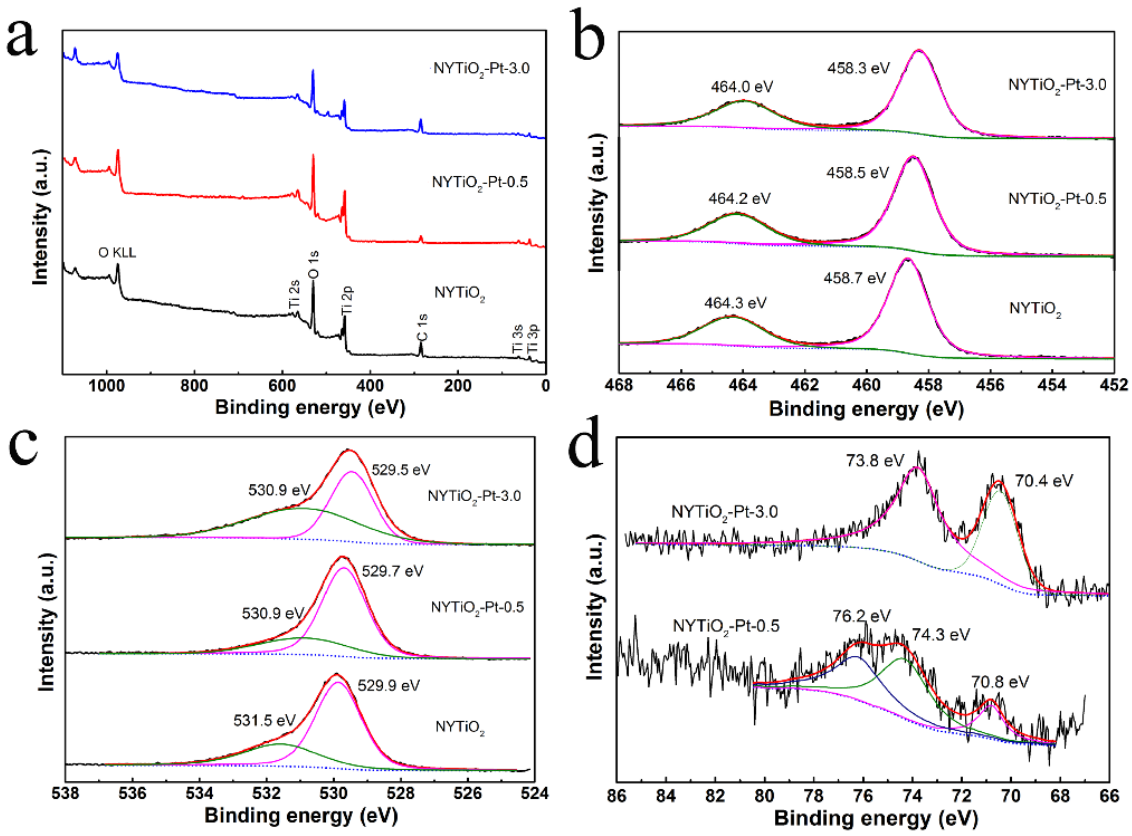

Figure 4. XPS spectra of $NYTiO_2$, $NYTiO_2$-Pt-0.5 and $NYTiO_2$-Pt-3.0: (a) full-range spectra, (b) Ti 2p, (c) O 1s and (d) Pt 4f.

X-ray photoelectron spectroscopy (XPS) is used to investigate the surface chemical states of the elements before and after Pt deposition. Figure 4a shows the full range spectra of $NYTiO_2$, $NYTiO_2$-Pt-0.5 and $NYTiO_2$-Pt-3.0. For $NYTiO_2$, the characteristic binding energies of Ti $2p_{3/2}$ and $2p_{1/2}$ are observed at 458.7 and 464.3 eV, respectively (Figure 4b), confirming the presence of Ti^{4+}.[37] The O 1s signal can be fitted into two symmetric peaks at 529.9 and 531.6 eV as illustrated in Figure 4c, corresponding to lattice oxygen (Ti-O) and absorbed H_2O, respectively.[37] For $NYTiO_2$-Pt-0.5, the binding energies of O 1s are centered at 529.7 and 530.9 eV, corresponding to lattice oxygen (Ti-O) and surface hydroxyl groups (Ti-OH). The binding energies of Ti $2p_{3/2}$ and Ti $2p_{1/2}$ slightly shift to 458.5 and 464.2 eV, respectively. The binding energies of Ti $2p_{3/2}$, Ti $2p_{1/2}$ and O 1s (Ti-O) further shift to 458.3, 464.0 and 529.5 in $NYTiO_2$-Pt-3.0, respectively. The peak of surface hydroxyl groups (Ti-OH) can be observed at 530.9 eV in the O 1s spectrum of $NYTiO_2$-Pt-3.0. Figure 4d presents the Pt 4f spectra. For $NYTiO_2$-Pt-0.5, the peak position of Pt $4f_{7/2}$ is at 70.8 eV, corresponding to metallic Pt^0.[24, 38, 39] The peak positions of Pt $4f_{5/2}$ are observed at 74.3 and 76.2 eV, corresponding to metallic Pt^0 and oxidized Pt^{2+}, respectively, indicating the coexistence of Pt^0 and Pt^{2+} species in the Pt nanoclusters [24, 38, 39]. For $NYTiO_2$-Pt-3.0, the peak positions of Pt $4f_{7/2}$ and $4f_{5/2}$ are 70.4 and 73.8 eV, respectively, indicating the existence of only metallic Pt^0 species. Namely, there is Pt-O-Ti bond between Pt nanoclusters and TiO_2 in $NYTiO_2$-Pt-0.5. Further, the presence of oxidized Pt^{2+} species is conducive to H_2 production via suppressing the hydrogen oxidation in the photocatalytic water splitting.[31, 38] The peaks of Pt $4f_{7/2}$ and $4f_{5/2}$ for $NYTiO_2$-Pt-3.0 are more obvious, due to the higher Pt

content, leading to a better signal-to-noise ratio.

From the XPS results and discussion, one can see that the negative shifts of Ti 2p and O 1s after NaOH-modification accompanying with Pt deposition can be attributed to two reasons. First, Pt nanoclusters have high ability to trap electrons, leading to higher negative shift of Ti 2p and O 1s in NYTiO_2-Pt-3.0 than in NYTiO_2-Pt-0.5. On the other hand, the NaOH-modification of the TiO_2 surface can induce the surface hydroxyl groups to bring a negative shift in the binding energies of Ti 2p and O 1s.[40]

XPS results show that the NYTiO_2-Pt-0.5 presents metallic Pt^0 and oxidized Pt^{2+} species, while the NYTiO_2-Pt-3.0 possesses only metallic Pt^0 species. This means that NaOH-modification can induce both metallic Pt^0 and oxidized Pt^{2+} species at low Pt content and only metallic Pt^0 species at high Pt content in NYTiO_2-Pt. Most possibly, at high Pt content, NaOH can not retard the reduction speed of H_2PtCl_6, leading to only metallic Pt^0 species. However, at low Pt content, NaOH can effectively retard the Pt nanocrystallites growth via decreasing the reduction speed of H_2PtCl_6, resulting in both metallic Pt^0 and oxidized Pt^{2+} species in Pt nanoclusters. In addition, this NaOH modification process also leads to numerious hydroxyls groups attached on TiO_2 surface, which is also helpful for highly dispersed ultrafine Pt nanoclusters. The metallic Pt^0 species adsorbed on the TiO_2 surface can serve as the active sites trapping photogenerated electrons and facilitate H_2 evolution.[24, 41] And oxidized Pt^{2+} species embedded in NYTiO_2-Pt can take the role of the photocatalytically active sites and limit the fast backward reaction of H_2 and O_2.[38, 39] Thus,

although NYTiO$_2$-Pt-0.5 has lower Pt content, it may demonstrate higher H_2 evolution rate than that demonstrated by NYTiO$_2$-Pt-3.0 due to the co-existence of Pt^0 and Pt^{2+} species.

The photocatalytic H_2 production performance of the NYTiO$_2$-Pt samples is then evaluated in methanol/water mixture under simulated solar light. Figure 5a depicts the H_2 production profiles of the NYTiO$_2$-Pt samples in 5 h. It shows that NYTiO$_2$-Pt-0.5 has the best performance of photocatalytic H_2 production, with 104.38 mmol g^{-1} in 5 h, consistent with our argument. On the contrary, NYTiO$_2$-Pt-3.0 demonstrates the worst performance, with only 1.22 mmol g^{-1} in 5h. Figure 5b presents the H_2 production rates of the NYTiO$_2$-Pt samples. The NYTiO$_2$-Pt-3.0 with the highest Pt content produces hydrogen at a rate of 0.24 mmol h^{-1} g^{-1}. The H_2 evolution rate increases to 0.64 mmol h^{-1} g^{-1} for NYTiO$_2$-Pt-2.0 and jumps to 16.50 mmol h^{-1} g^{-1} for NYTiO$_2$-Pt-1.0, 25.8 times comparing to that produced by NYTiO$_2$-Pt-2.0. We observe even further increase up to 20.88 mmol h^{-1} g^{-1} for NYTiO$_2$-Pt-0.5, before it drops to 14.06 mmol h^{-1} g^{-1} for NYTiO$_2$-Pt-0.25. These indicate that NYTiO$_2$-Pt-0.5 contains optimal Pt content. Comparing to pure NYTiO$_2$ (Figure S6), all the NYTiO$_2$-Pt samples perform significantly better photocatalytic activities under the same water splitting reaction conditions. Furthermore, irradiation under a monochromatic light at 365 nm, NYTiO$_2$-Pt-0.5 demonstrates a H_2-evolution rate of 4.71 mmol h^{-1} g^{-1}, corresponding to an apparent quantum yield (AQY) value of ~85.6%, which is higher than many previously reported TiO$_2$-Pt photocatalysts.[42-45] Such strong photocatalytic performance is attributed to the unique yolk-shell structure for effective light harvesting and uniformly anchored Pt nanoclusters with metallic Pt^0 and oxidized Pt^{2+} species.

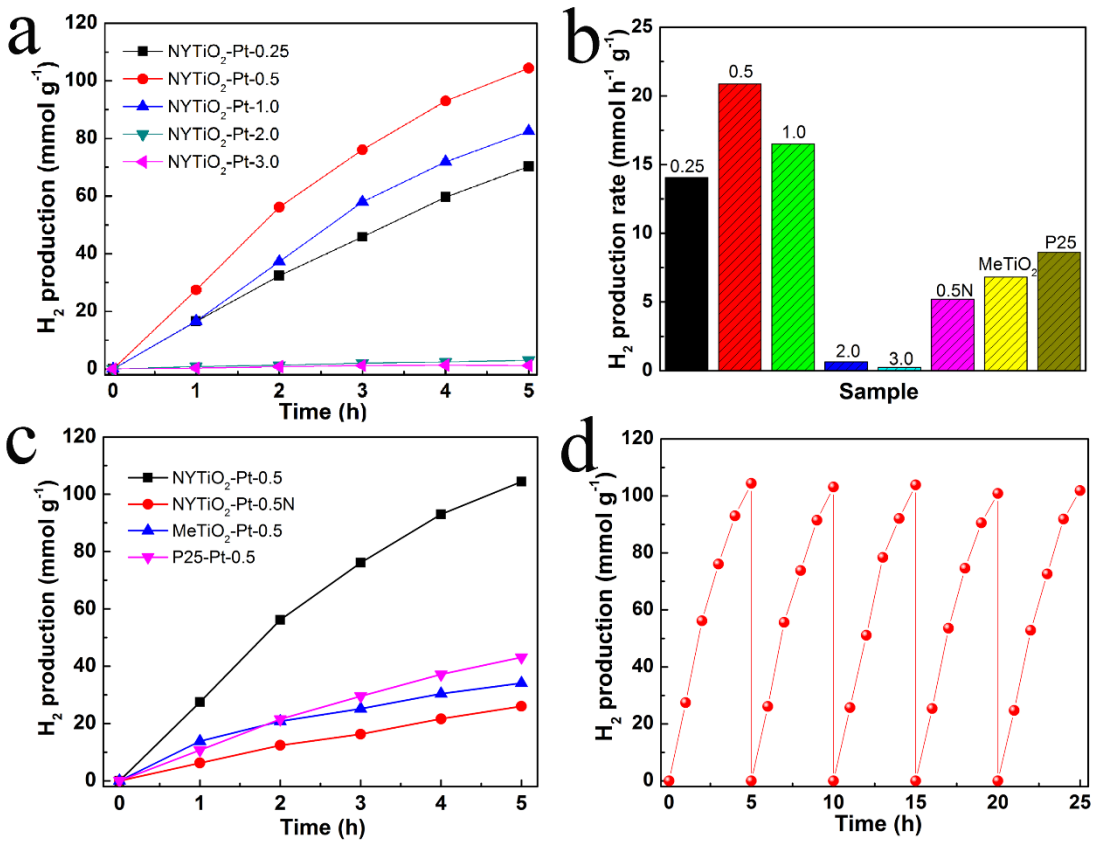

Figure 5. (a) H_2 production profiles of the $NYTiO_2$-Pt samples, (b) H_2 production rates of all the samples, (c) H_2 production profiles of $NYTiO_2$-Pt-0.5, $NYTiO_2$-Pt-0.5N, $MeTiO_2$-0.5 and P25-Pt-0.5 with the same Pt content and (d) cycle performance of H_2 production of $NYTiO_2$-Pt-0.5.

To investigate the effect of NaOH modification, 0.188 wt% Pt in $NYTiO_2$ photocatalyst without NaOH treatment (designated as $NYTiO_2$-Pt-0.5N) is prepared through a $NaBH_4$-reduction process of H_2PtCl_6 in a neutral environment. Figure 5c presents the photocatalytic H_2 production performance of $NYTiO_2$-Pt-0.5N in 5h. It clearly shows that the H_2 evolution rate of $NYTiO_2$-Pt-0.5 is 4 times that from $NYTiO_2$-Pt-0.5N (5.20 mmol h^{-1} g^{-1}). This means that the NaOH modification of $NYTiO_2$-Pt photocatalyst significantly improves its photocatalytic activity.

To further verify the role of hierarchical nanosheet-constructed yolk-shell structure for

light harvesting, mesoporous TiO_2 ($MeTiO_2$) microspheres are synthesized and utilized for photocatalytic H_2 production at the same condition. The anatase nanoparticle constructed $MeTiO_2$ porous microspheres exhibit a BET specific surface area of 82.1 m^2 g^{-1} and an average pore size of ~9 nm (Figure S7-S9). The 0.188 wt% Pt in $MeTiO_2$ photocatalyst (designated as $MeTiO_2$-Pt-0.5) is prepared with the same procedure for $NYTiO_2$-Pt-0.5. However, the $MeTiO_2$-Pt-0.5 only demonstrates a H_2 production rate of 6.81 mmol h^{-1} g^{-1}, only 32.6% of the H_2 production rate of $NYTiO_2$-Pt-0.5 (Figure 5b and 5c). The commercial P25 nanoparticles are also loaded with 0.188 wt% Pt (designated as P25-Pt-0.5) for photocatalytic H_2 production at the same condition. Figure S10 shows the XRD and HRTEM images of P25-Pt-0.5, confirming the existence of anatase-rutile phase and Pt nanoclusters. Figure S11 also displays the UV-Vis absorption spectrum of P25-Pt-0.5. Table 1 lists its electronic band gap, similar to those of other samples. The prepared P25-Pt-0.5 presents a H_2 production rate of 8.62 mmol h^{-1} g^{-1}, only 41.3% of the H_2 production rate of $NYTiO_2$-Pt-0.5 (Figure 5b and 5c). These confirm that the nanosheet-constructed yolk-shell structure is favorable for effective light harvesting (Scheme 1b), thus enhancing the photocatalytic H_2 production.

Since the $NYTiO_2$-Pt-0.5 is synthesized under alkaline environment, the surfaces of Pt nanoclusters are surrounded by numerous hydroxyl groups.[31] This retards the H_2PtCl_6 reduction as well as the growth and aggregation of Pt nanoclusters, resulting in co-existence of metallic Pt^0 and oxidized Pt^{2+} species.[24] The metallic Pt^0 species acts as electron trapping reservoirs to effectively separate photogenerated electron-hole pairs. The oxidized Pt^{2+}

species can efficiently prevent the backward reaction of H_2 and O_2. Meanwhile, the surface of TiO_2 nanosheets is also modified by the hydroxyl groups to introduce active sites for Pt deposition, leading to uniform and ultrafine Pt nanoclusters strongly anchoring onto the surface of TiO_2 nanosheets in the NYTiO_2 shell. Since the photocatalytic H_2 production reaction occurs at the interface of TiO_2 and Pt,[24] the NaOH-modified ~0.6 nm Pt nanoclusters anchoring onto NYTiO_2-Pt-0.5 can essentially improve the H_2 production.

The stability of the NYTiO_2-Pt-0.5 for the photocatalytic H_2 evolution is evaluated through cycling H_2 production (Figure 5d). No obvious decrease in the photocatalytic activity after 5 cycles (25 h) is observed, indicating very good stability of NYTiO_2-Pt-0.5. The good stability of NYTiO_2-Pt-0.5 catalyst is attributed to the numerous hydroxyl group, strong Pt-O-Ti bond, ultrafine size and good dispersion of Pt nanoclusters as shown in Scheme 1b. XPS is further employed to investigate the structural stability of NYTiO_2-Pt-0.5 after 25 h reaction (designated as NYTiO_2-Pt-0.5H); see Figure S12. One can see that after 25 h of photocatalytic reaction, there is no obvious difference between NYTiO_2-Pt-0.5 and NYTiO_2-Pt-0.5H except for the noise signal increase for Pt. We speculate that this increase of noise signals is induced by more hydroxyls groups attached on TiO_2 and Pt nanoclusters. More detailed investigation is required to verify this.

Conclusions

In summary, we have designed an alkali-modified NYTiO_2-Pt light harvesting reactor for highly efficient photocatalytic H_2 production. The Pt nanoclusters are uniformly deposited

through a simultaneous $NaBH_4$ reduction of H_2PtCl_4 and NaOH-modification in an alkaline environment. The porous, nanosheet-based yolk-shell microspherical TiO_2, co-catalysing with highly dispersed ~0.6 nm Pt nanoclusters with metallic Pt^0 and oxidized Pt^{2+} species in a low content of 0.188 wt% Pt, demonstrates excellent photocatalytic stability and up to 20.88 mmol h^{-1} g^{-1} H_2 production under simulated solar light. We believe that our demonstration here provides a simple, efficient and economic route to decorate metal oxides-based photocatalysts with ultrafine noble metal nanoclusters for highly efficient solar energy assisted water splitting at a very low content of noble metal. On the basis of these findings, other efficient light harvesting systems with a facile alkali modification might be further developed for highly photocatalytic H_2 production.

Acknowledgments

B. L. Su acknowledges the Chinese Central Government for an "Expert of the State" position in the Program of the "Thousand Talents" and a Life Membership at the Clare Hall, Cambridge and the financial support of the Department of Chemistry, University of Cambridge. Y. Li acknowledges Hubei Provincial Department of Education for the "Chutian Scholar" program. T. H. acknowledges support from the Royal Academy of Engineering through a Research Fellowship and an EPSRC Impact acceleration grant. This work is supported by the National Key Research and Development Program of China (2016YFA0202602), Program for Changjiang Scholars and Innovative Research Team in University (IRT_15R52), International Science & Technology Cooperation Program of China

(2015DFE52870), National Natural Science Foundation of China (51302204 and 51502225) and the Fundamental Research Funds for the Central Universities (WUT: 2016ⅢⅠ029).

Appendix A. Supporting information

Part of the materials characterizations.

References

[1] X. Chen, S. Shen, L. Guo, S.S. Mao, Chem. Rev., 110 (2010) 6503-6570.

[2] M. Murdoch, G.I.N. Waterhouse, M.A. Nadeem, J.B. Metson, M.A. Keane, R.F. Howe, J. Llorca, H. Idriss, Nat. Chem., 3 (2011) 489-492.

[3] A. Patsoura, D.I. Kondarides, X.E. Verykios, Appl. Catal. B: Environ., 64 (2006) 171-179.

[4] W.J. Ong, L.L. Tan, S.P. Chai, S.T. Yong, A.R. Mohamed, ChemSusChem, 7 (2014) 690-719.

[5] A.U. Pawar, C.W. Kim, M.J. Kang, Y.S. Kang, Nano Energy, 20 (2016) 156-167.

[6] X. Chen, L. Liu, Y.Y. Peter, S.S. Mao, Science, 331 (2011) 746-750.

[7] Q. Li, B. Guo, J. Yu, J. Ran, B. Zhang, H. Yan, J.R. Gong, J. Am. Chem. Soc., 133 (2011) 10878-10884.

[8] L. Zhang, C. Baumanis, L. Robben, T. Kandiel, D. Bahnemann, Small, 7 (2011) 2714-2720.

[9] J. Sun, J. Zhang, M. Zhang, M. Antonietti, X. Fu, X. Wang, Nat. Commun., 3 (2012)

1139.

[10] F. Wang, C. Di Valentin, G. Pacchioni, J. Phys. Chem. C, 116 (2012) 8901-8909.

[11] A. Kubacka, M. Fernández-García, G. Colón, Chem. Rev., 112 (2011) 1555-1614.

[12] C. Wang, L. Wang, J. Jin, J. Liu, Y. Li, M. Wu, L. Chen, B. Wang, X. Yang, B.L. Su, Appl. Catal. B: Environ., 188 (2016) 351-359.

[13] Z. Zhang, W. Li, M.F. Yuen, T.-W. Ng, Y. Tang, C.-S. Lee, X. Chen, W. Zhang, Nano Energy, 18 (2015) 196-204.

[14] A. Samokhvalov, Renew. Sust. Energy Rev., 72 (2017) 981-1000.

[15] Y. L. Lee, C.F. Chi, S.Y. Liau, Chem. Mater., 22 (2009) 922-927.

[16] L. Zhu, M. Hong, G.W. Ho, Nano Energy, 11 (2015) 28-37.

[17] X. Yu, J. Zhang, Z. Zhao, W. Guo, J. Qiu, X. Mou, A. Li, J.P. Claverie, H. Liu, Nano Energy, 16 (2015) 207-217.

[18] G. Li, Z. Lian, W. Wang, D. Zhang, H. Li, Nano Energy, 19 (2016) 446-454.

[19] J.M. Valero, S. Obregón, G. Colón, ACS Catal., 4 (2014) 3320-3329.

[20] J. Yu, G. Dai, B. Huang, J. Phys. Chem. C, 113 (2009) 16394-16401.

[21] H. Zhao, M. Wu, J. Liu, Z. Deng, Y. Li, B.L. Su, Appl. Catal. B: Environ., 184 (2016) 182-190.

[22] X. Li, J. Yu, J. Low, Y. Fang, J. Xiao, X. Chen, J. Mater. Chem. A, 3 (2015) 2485-2534.

[23] W.Y. Teoh, L. Mädler, R. Amal, J. Catal., 251 (2007) 271-280.

[24] F.C. Wang, C.H. Liu, C.W. Liu, J.H. Chao, C.H. Lin, J. Phys. Chem. C, 113 (2009) 13832-13840.

[25] H.S. Kibombo, C.M. Wu, R. Peng, J. Baltrusaitis, R.T. Koodali, Appl. Catal. B: Environ., 136 (2013) 248-259.

[26] X. Li, W. Bi, L. Zhang, S. Tao, W. Chu, Q. Zhang, Y. Luo, C. Wu, Y. Xie, Adv. Mater., 28 (2016) 2427-2431.

[27] B.S. Huang, F.Y. Chang, M.Y. Wey, Int. J. Hydrogen Energy, 35 (2010) 7699-7705.

[28] M.P. Languer, F.R. Scheffer, A.F. Feil, D.L. Baptista, P. Migowski, G.J. Machado, D.P. de Moraes, J. Dupont, S.R. Teixeira, D.E. Weibel, Int. J. Hydrogen Energy, 38 (2013) 14440-14450.

[29] B. Zhu, K. Li, S. Wang, S. Zhang, S. Wu, W. Huang, J. Dispersion Sci. Technol., 29 (2008) 1408-1411.

[30] X. Meng, S. Ouyang, T. Kako, P. Li, Q. Yu, T. Wang, J. Ye, Chem. Commun., 50 (2014) 11517-11519.

[31] Y. Zhai, D. Pierre, R. Si, W. Deng, P. Ferrin, A.U. Nilekar, G. Peng, J.A. Herron, D.C. Bell, Science, 329 (2010) 1633-1636.

[32] C.T. Dinh, H. Yen, F. Kleitz, T.O. Do, Angew. Chem. Int. Ed., 53 (2014) 6618-6623.

[33] J. Yu, Y. Hai, B. Cheng, J. Phys. Chem. C, 115 (2011) 4953-4958.

[34] Y. Li, Z.Y. Fu, B.L. Su, Adv. Funct. Mater., 22 (2012) 4634-4667.

[35] X. Wang, J.C. Yu, C. Ho, Y. Hou, X. Fu, Langmuir, 21 (2005) 2552-2559.

[36] J. Jin, S.Z. Huang, Y. Li, H. Tian, H.E. Wang, Y. Yu, L.H. Chen, T. Hasan, B.L. Su, Nanoscale, 7 (2015) 12979-12989.

[37] Z. Zhang, Z. Wang, S.W. Cao, C. Xue, J. Phys. Chem. C, 117 (2013) 25939-25947.

[38] Y. Hang Li, J. Xing, Z. Jia Chen, Z. Li, F. Tian, L. Rong Zheng, H. Feng Wang, P. Hu, H. Jun Zhao, H. Gui Yang, Nat. Commun., 4 (2013) 2500.

[39] J. Xing, H.B. Jiang, J.F. Chen, Y.H. Li, L. Wu, S. Yang, L.R. Zheng, H.F. Wang, P. Hu, H.J. Zhao, H.G. Yang, J. Mater. Chem. A, 1 (2013) 15258-15264.

[40] J. Yu, X. Li, Z. Xu, W. Xiao, Environ. Sci. Technol., 47 (2013) 9928-9933.

[41] H.S. Kibombo, C.M. Wu, R. Peng, J. Baltrusaitis, R.T. Koodali, Appl. Catal. B: Environ., 136–137 (2013) 248-259.

[42] H. Zhou, X. Li, T. Fan, F.E. Osterloh, J. Ding, E.M. Sabio, D. Zhang, Q. Guo, Adv. Mater., 22 (2010) 951-956.

[43] A.A. Melvin, K. Illath, T. Das, T. Raja, S. Bhattacharyya, C.S. Gopinath, Nanoscale, 7 (2015) 13477-13488.

[44] J. Liu, G. Liu, M. Li, W. Shen, Z. Liu, J. Wang, J. Zhao, L. Jiang, Y. Song, Energy Environ. Sci., 3 (2010) 1503-1506.

[45] C. Yang, Z. Wang, T. Lin, H. Yin, X. Lü, D. Wan, T. Xu, C. Zheng, J. Lin, F. Huang, J. Am. Chem. Soc. 135 (2013) 17831-17838.

Jun Jin received the Ph. D. degree in 2015 under the supervision of Prof. Dr. Bao-Lian Su and Prof. Dr. Yu Li from Wuhan University of Technology, China. Currently, he is a Postdoctoral Research Fellow at Nanyang Technological University, Singapore. His research interests focus on designing novel nanomaterials for energy conversion and storage.

Chao Wang obtained the Master of Engineering degree in 2013 from Wuhan University of Technology, China. He is pursuing his Ph.D. degree under the guidance of Prof. Bao-Lian Su and Prof. Yu Li at State Key Laboratory of Advanced Technology for Materials Synthesis and Processing, Wuhan University of Technology, China. His current research involves developing techniques for advanced microscopy and the synthesis of organic-inorganic metal sulfide nanomaterials for photocatalysis applications and their antiphotocorrosion mechanism.

Xiao-Ning Ren received the Bachelor degree in Inorganic Non-Metallic Materials Engineering in 2011 from Wuhan University of Technology. She is pursuing her Ph. D. degree under the guidance of Prof. Bao-Lian Su and Prof. Yu Li at State Key Laboratory of Advanced Technology for Materials Synthesis and Processing, Wuhan University of Technology, China. Her current research interests are mainly focused on designing novel nanomaterials for photocatalysis application.

Shaozhuan Huang received his Ph. D. degree in Materials Physics and Chemistry under the supervision of Prof. Dr. Bao-Lian Su and Prof. Dr. Yu Li from Wuhan University of Technology in 2015. Then he worked as a postdoctoral researcher in in Leibniz Institute for Solid State and Materials Research (IFW Dresden), Germany. He is currently a research assistant in Singapore University of Technology and Design (SUTD), Singapore. His current research interests are mainly focused on designing novel materials for electrochemical energy conversion and storage.

Min Wu received her Ph. D. in Physics from Institute of Photonics, University of Strathclyde, UK in 2010 and went to the University of Namur as a post-doctoral researcher in CMI Laboratory with Prof. Bao-Lian Su after. Currently, she is a Professor in Wuhan University of Technology and her research interests are inorganic semiconductor nanomaterials photonic crystals design and synthesis for photosynthesis and photocatalysis in environment and energy fields.

Li-Hua Chen awarded his Ph. D. degrees, one in inorganic chemistry from Jilin University, China (2009), and another in inorganic materials chemistry from University of Namur, FUNDP, Belgium (2011). He is currently a full professor working in the State Key Laboratory of Advanced Technology for Materials Synthesis and Processing from the Wuhan University of Technology, China. His research is aimed at new porous materials with designed hierarchically porosity towards catalysis.

Bin-Jie Wang received his Ph. D. degree of Physics at Electron Microscopy for Materials Science (EMAT) Laboratory of Physics Department in University of Antwerp in 2007 and 2011 respectively. Most of his PhD work was done under the supervision of Profs. Dominique Schryvers and Hosni Idrissi. Currently, he works in the leading APR TEM application team at FEI Company in Shanghai. His main research interests are TEM techniques application on material science and plasticity mechanisms in metals and alloys.

Tawfique Hasan gained his PhD from the University of Cambridge in 2009. He is currently a University Lecturer in Electronic Materials and Devices, Deputy Director for Teaching and Training of the EPSRC funded Centre for Doctoral Training in Graphene Technology and Director of the MRes program in Graphene Technology at the Cambridge Graphene Centre, Cambridge University Engineering Department. His current research focuses on formulation

of functional inks of 0, 1- and 2-dimensional nanomaterials and their hybrids for a wide range of printable and flexible device applications including ultrafast lasers, photonic, (opto)electronic and energy devices. He is a Title A Fellow of Churchill College, Cambridge and currently holds a prestigious Royal Academy of Engineering Research Fellowship.

Prof. Yu Li received his Bachelor degree from Xi'an Jiaotong University in 1999 and received his Mater degree from Liaoning Shihua University in 2002. He obtained his Ph.D. from Zhejiang University in 2005. He worked in EMAT at the University of Antwerp with Prof. G. Van Tendeloo in 2005 and then in CMI at the University of Namur with Prof. Bao-Lian Su in 2006. Currently, he is a "Chutian" Professor at Wuhan University of Technology. His research interests include nanomaterials design and synthesis, hierarchically porous materials synthesis, and their applications in the fundamental aspects of energy and environment.

Prof. Bao-Lian Su created the Laboratory of Inorganic Materials Chemistry (CMI) at the University of Namur, Belgium in 1995. He is currently Full Professor of Chemistry, Member of the Royal Academy of Belgium, Fellow of the Royal Society of Chemistry, UK and Life Member of Clare Hall College, University of Cambridge. He is also Changjiang Professor at Wuhan University of Technology and an ‘‘Expert of the State’’ in the frame of ‘‘Thousands Talents’’ program, China. His current research fields include the synthesis, the property study and the molecular engineering of organized, hierarchically porous and bio-inspired materials, living materials and leaf-like materials and the immobilization of bio-organisms for artificial photosynthesis, (photo) Catalysis, Energy Conversion and Storage, Biotechnology, Cell therapy and Biomedical applications.